Clays and Clay Minerals, Vol. 65, No. 3, 193–205, 2017.

KAOLINITE AGGREGATION IN BOOK-LIKE STRUCTURES FROM NON-AQUEOUS MEDIA

ROLA MANSA, GUY B. NGASSA PIEGANG, AND CHRISTIAN DETELLIER*

Center for Catalysis Research and Innovation and Department of Chemistry and Biomolecular Sciences, University of Ottawa, Ottawa, Ontario K1N 6N5, Canada

Abstract—To control a vast spectrum of applications and processes, an understanding of the morphologies of clay mineral assemblies dispersed in aqueous or non-aqueous media is important. As such, the objective of this study was to verify the relationship between dispersion medium type and the size and morphology of the clay aggregates that are formed, which can increase knowledge on the assembly formation process. Scanning electron microscopy (SEM), X-ray diffraction (XRD), and Fourier-transform infrared (FTIR) spectroscopy were used in an attempt to describe kaolinite platelet organization in non-aqueous media and to compare it to the organization in aqueous media or in media with or without a selection of dissolved organic polymers. The SEM images indicated that the kaolinite platelet assembly process occurs during slow evaporation of the solvent. Because the experimental procedure was rigorously identical for all cases in this study, the SEM images compared how the effects of various media and environments on kaolinite platelet interactions can lead to different morphologies. Quite spectacular morphological differences were indeed observed between samples dispersed in aqueous and non-aqueous media, particularly when the kaolinite platelets were dispersed in an organic solvent with dissolved organic polymers. For kaolinite dispersed in water, only small aggregates were observed after slow evaporation. In contrast, large kaolinite booklets or vermiform aggregates were formed by slow solvent evaporation when kaolinite was first dispersed into some organic solvents. The aggregates were particularly large when an organic polymer was dissolved in the organic solvent. For example, kaolinite aggregates dispersed in a binary cyclohexane/toluene mixture with dissolved ethyl cellulose (EC) had top apparent surface areas (*i.e.* stacking length × width) of more than 3,000 μm^2. Other dissolved polymers, such as polystyrene or the polysaccharide, guar gum, gave similar results. Kaolinite platelet aggregation resulted from face-to-face interactions as well as edge-to-face and edge-to-edge interactions. The XRD results showed that ethyl cellulose led to the formation of smaller kaolinite platelets with an increased tendency to form larger aggregates, which is due to the ability of EC to chemically interact with silanol and/or the aluminol groups of kaolinite.

Key Words—Aggregation, Aqueous Media, Booklets, Kaolinite, Morphology, Non-aqueous Media, Organic Solvent, Platelet, Polymer, Vermiform Structure.

INTRODUCTION

Kaolinite is one of the polytypes of the kaolin subgroup and the structure consists of dioctahedral 1:1 layers with the general composition $Al_2Si_2O_5(OH)_4$ (Brigatti *et al*., 2013). This structure is highly asymmetric, has strong dipolar interactions between the layers, and has a network of H-bonds between the aluminol groups of the octahedral sheet and the siloxane groups of the tetrahedral sheet (Giese, 1982; Detellier and Schoonheydt, 2014). Consequently, the 1:1 layers are stacked to form individual particles or platelets that are usually pseudo-hexagonal and typically made of about 50−200 layers with a thickness on the order of 40 to 100 nm (Johnston, 2010). The platelets can be considered as individual crystals of kaolinite. The solid phase morphology of kaolinite results from the several ways that platelets can be arranged in macrostructures. In particular, the kaolinite platelets can be stacked, piled into much larger aggregates to form booklets, or in some cases arranged into a worm-like, vermiform morphology similar to what is commonly observed for vermiculite. Kaolin booklets formed into vermiform aggregates are common and well known in kaolin deposits (Psyrillos *et al.*, 1999; Christidis, 2013; Wilson *et al*., 2014). The kaolinization of biotite commonly occurs in soils and results in sand-sized kaolinite pseudomorphs (Rebertus *et al.*, 1986). Of particular interest is the progressive morphological changes from a vermiform morphology to a blocky morphology as burial depth is increased and corresponds to the progressive replacement of kaolinite with dickite in sedimentary basins during diagenesis (Beaufort *et al*., 1998; Kameda *et al*., 2008). Vermiform kaolin aggregates can have a range of sizes and morphologies. For example, in one sample analyzed by Kameda *et al.* (2008), lamellar crystals were piled up almost parallel to each other and assembled into wider assemblies. These large structures can be several hundreds of micrometers long (Kameda *et al*., 2008). The assumption that the structures result from face-to-face contacts between kaolinite platelets due to siloxane and aluminol surface interactions is plausible. The piles

* E-mail address of corresponding author:
dete@uottawa.ca
DOI:10.1346/CCMN.2017.064059

of kaolinite platelets are then assembled edge-to-edge to form larger structures. Some pseudo-hexagonal crystals linked edge-to-face to the large structure were also detected on the sides. At pH 5.5, aqueous kaolinite suspensions have edges that contain silanol and hydrated aluminol groups with aqueous pKa values of 6.9 and 5.7, respectively (pKa values calculated using the first principles molecular dynamics method). These pKa values are in the range of several previously measured values (Liu *et al.*, 2013). While the siloxane and aluminol basal surfaces play the main role in piling kaolinite platelets; edge-to-face and edge-to-edge interactions involve both silanol groups and aluminol groups. The 1:1 structure can have a low permanent charge due to some isomorphic substitutions or to small amounts of expandable clay minerals, and both could play a minor role in these platelet assemblies. Recently, an estimated surface charge density of 25 nC/cm^2 for kaolinite layers was calculated using electrostatic force microscopy (EFM) measurements (Liu *et al.*, 2015a). Given the prominent role kaolinite plays in human activities (Schroeder and Erickson, 2014), the current incomplete understanding of clay mineral assembly morphologies in aqueous or non-aqueous media is a vital missing link for better control of a vast spectrum of applications and processes, such as catalysis and organic reactivity (Laszlo, 1986; Mccabe and Adams, 2013; Ngnie *et al.*, 2016), clay-polymer nanocomposites (Galimberti *et al.*, 2013; Dedzo and Detellier, 2016), bitumen extraction from oil sands (Detellier *et al.*, 2015; Lin *et al.*, 2016), soil permeability and soil transport processes (Yong and Mourato, 1990), or the abiotic origin of life (Brack, 2013). The purpose of the present study was to fill this gap by analyzing and comparing the organization of kaolinite platelets in non-aqueous and aqueous media and in the presence of a selection of organic polymers, primarily using scanning electron microscopy (SEM) and X-ray diffraction (XRD) techniques.

MATERIALS AND METHODS

Materials

The KGa-1b (Georgia) kaolinite was obtained from the Source Clays Repository of The Clay Minerals Society. The KGa-1b kaolinite from the Buffalo China Mines in the Buffalo Creek formation is classified as a soft kaolin and is mainly associated with Coastal Plain sediments of Cretaceous age. The particle size distribution of KGa-1b was determined to be 57.8% <2 μm and 32.0% <0.5 μm (Pruett and Webb, 1993). The kaolinite crystals in KGa-1b occur as large, euhedral, interlocking plates and as vermiform crystals; the organic matter content is 0.04–0.10% (Moll, 2001). The Cretaceous kaolins generally contain a number of vermicular crystals with some books and plates (Murray and Keller, 1993). The KGa-1b kaolinite has a low permanent charge of 0.6 meq/100 g (Aung *et al.*, 2015). Toluene (99.9%) and ethanol (99%) were obtained from Fisher Scientific (Pittsburgh, Pennsylvania, USA). Cyclohexane (Chromasolv for HPLC, >99.9%), polystyrene (average M_w ~280,000 by GPC), polycaprolactone diol (average M_n ~530), guar gum (loss on drying $\leqslant$ 13%; total ash $\leqslant$ 1%), and ethyl cellulose (48% ethoxy) were all obtained from Sigma-Aldrich (St. Louis, Missouri, USA) and used as received. Deionized water was prepared and used in the experiments.

Methods

Images of the samples were taken at magnifications that ranged from 400 to 20,000× using a JSM-7500F FESEM (JEOL, Tokyo, Japan) scanning electron microscope (SEM) operated at an accelerating voltage of 2, 3, or 5 kV depending on the sample. The aggregates observed in the SEM images were statistically analyzed. Aggregates were defined as collections of particles with a minimum stacking length (length parallel to the stacking direction) of 1 μm. Measurements of the stacking length and width of an aggregate were made using Image J software (U. S. National Institutes of Health, Bethesda, Maryland, USA). Only the aggregates that could be observed to show a lateral view of the stacked particles were considered. Although this invariably excluded other aggregates with only a top view observed, images at both low and high magnifications were analyzed to ensure that a sufficient number of clay particles and aggregates were included to decrease the likelihood of unsampled populations. X-ray diffraction (XRD) patterns were obtained using a Rigaku Ultima IV diffractometer (Rigaku, Tokyo, Japan) with Cu Kα radiation (λ = 1.5406 Å) operated at 40 kV and 44 mA with a scan rate of 2.0º2θ min^{-1}. Fourier-transform infrared attenuated total reflectance (FTIR-ATR) spectra were recorded at room temperature on a Nicolet 6700 FTIR spectrometer (Thermo Fisher Scientific, Waltham, Massachusetts, USA) equipped with OMNIC software in attenuated total reflection mode using the SMART diamond ATR attachment in the 4500 to 650 cm^{-1}range with a resolution of 4 cm^{-1}.

Procedure for the preparation of the SEM samples

KGa-1b (0.3g) was added to a selected amount of solvent or a solvent mixture. Under aqueous and ethanolic conditions, the specified amount of kaolinite was added to the following solvent/solvent mixtures: (a) 15 mL of water, (b) 37.5 mL of water and 11.25 mL of ethanol, or (c) 6.5 mL of ethanol. Under aqueous and ethanolic conditions and in the presence of a polymer, kaolinite was added to the following solvent/solvent mixtures: (a) 15 mL of water with 0.05 g of previously dissolved guar gum, or (b) 37.5 mL of water and 0.075 g of ethyl cellulose previously dissolved in 11.25 mL of ethanol. Under non-aqueous conditions, kaolinite was added to the following solvent/solvent mixtures: (a) 5 mL

https://doi.org/10.1346/CCMN.2017.064059 Published online by Cambridge University Press

of cyclohexane and 1.5 mL of toluene, (b) 5 mL of cyclohexane and 4.5 mL of toluene, (c) 5 mL of cyclohexane and 9 mL of toluene, or (d) 6.5 ml of toluene. Under non-aqueous conditions and in the presence of a polymer, kaolinite was added to the following solvent/solvent mixtures: (a) 5 mL of cyclohexane and 0.075 g of polystyrene previously dissolved in 1.5 mL of toluene, (b) 5 mL of cyclohexane and 0.075 g of ethyl cellulose previously dissolved in 1.5 mL of toluene, (c) 5 mL of cyclohexane and 0.225 g of ethyl cellulose previously dissolved in 4.5 mL of toluene, or (d) 5 mL of cyclohexane and 0.45 g of ethyl cellulose previously dissolved in 9 mL of toluene. When a polymer was used, the amount of solvent depended on the solubility of the polymer. Blank experiments were done using the same amounts of solvent or co-solvent and clay as used in the actual experiments without the polymer. The sample suspensions were then mixed for 3 h at 385 rpm using a Thermo Scientific (ThermoFisher Scientific, Waltham, Massachusetts, USA) MaxQ 2000 benchtop orbital shaker and dried for 17 h in an oven at 58ºC to completely remove the solvent. In alternative experiments, samples were shaken for 3 h and then dried in an oven at 58ºC for 0, 4, and 7 h, which did not completely remove the solvent. The SEM images for the alternative experiment were obtained after a small aliquot of the sample was rapidly dried under atmospheric conditions. Also, the aggregates in the alternative experiment SEM images were defined for the statistical analyses to have a minimum stacking length of 3 μm. All of the SEM samples except one were coated with 5 nm of Au. A 7-nm Au coating was required for the K40_EC60 sample, which contained 0.45 g of ethyl cellulose for a solid component weight ratio of 40% kaolinite to 60% ethyl cellulose. Some mostly intact samples were broken into smaller pieces by hand and tended to be samples with greater polymer contents. For samples with a high polymer content, observing the clay particles was not possible unless the sample was broken into smaller pieces.

RESULTS AND DISCUSSION

To evaluate and assess kaolinite aggregation processes in various aqueous and non-aqueous media with and without polymers, a simple and reproducible procedure was designed and rigorously followed to prepare samples for SEM imaging. The SEM images were produced using dried solid materials and do not necessarily represent the morphology of the kaolinite particles dispersed in the solvent. Instead, the SEM images are representative of the assembly process which can occur during slow solvent evaporation. Consequently, the SEM images indicated that platelets interact in various media, which leads to different morphologies under different environments. Kaolinite dispersed in water formed only a few, small organized aggregates (Figures 1a, 1b). Kaolinite was dispersed in deionized water at pH 5.6 in the typical pH range used for kaolinite. The largest aggregate (Figure 1a) was 3.3 μm × 2.1 μm for a top surface area of 6.9 μm^2. The term "top surface area" is defined as the surface of one side of the aggregate and is the product of stacking length times the width. Kaolinite platelet associations were mainly edge-to-face as seen in another sample fraction (Figure 1b). The presence of both face-to-face and edge-to-face aggregations was consistent with Gupta *et al.* (2011) who used the same pH as the present study. At the suspension pH, the two kaolinite basal surfaces had positively charged alumina surfaces and negatively charged silica surfaces (Liu *et al*., 2015b), which drove the platelets to stack into aggregates. The kaolinite edges are made of silanol groups (pKa = 6.9) and hydrated aluminol groups (pKa = 5.7), which were calculated using a first principles molecular dynamics approach and these values are consistent with previous experimental

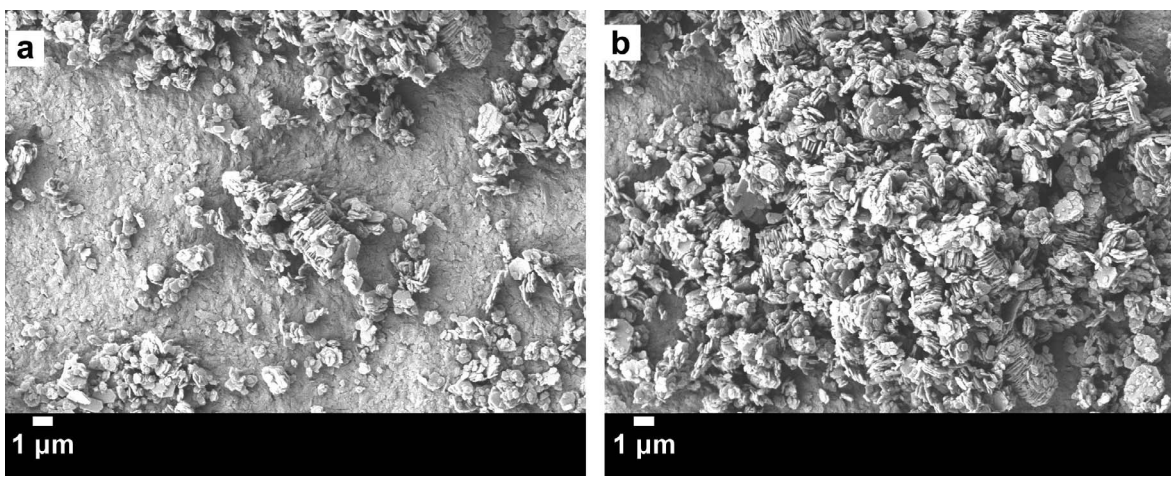

Figure 1. SEM micrographs (a, b) magnified 4,000 × for 0.3 g of kaolinite dispersed in 15 mL of water.

https://doi.org/10.1346/CCMN.2017.064059 Published online by Cambridge University Press

data (Liu *et al*., 2013). The silanol and hydrated aluminol chemical groups and the platelet aluminol and the siloxane basal surfaces are H-bonded to water and well hydrated, which restricts particle-particle interactions and results in relatively small aggregate dimensions. All of the observed aggregates were relatively small with 2.2 μm × 2.3 μm mean dimensions (width × stacking length) and mean areas of 6.0 μm^2 (Figure 2a), which was expected because particle-particle interactions are restricted under hydrated conditions. Hu *et al.* (2013) indicated that a colloidal suspension of kaolinite in aqueous dodecylamine was strongly aggregated during a hydrophobic agglomeration process. Can a water-soluble hydrophilic polymer, such as a polysaccharide, promote kaolinite aggregation by linking several platelets together? Guar Gum, a galactomannan polysaccharide obtained from the *Cyamopsis tetragonoloba* seed endosperm (Srivastava and Kapoor, 2005), was a good candidate polymer. Guar gum consists of a (1,4) β-D-manno-pyranosyl unit backbone linked at every second unit to a (1,6) α-D-galacto-pyranosyl unit (Figure 3a). Guar gum is used in many industrial applications which include use as a food additive. Moreover, guar gum was recently used to prepare bio-nanocomposites (Mansa and Detellier, 2013; Dziadkowiek *et al*., 2017). Much larger aggregates were indeed observed in a pH 6.3 aqueous solution that contained 14% guar gum (Figure 4a). The mean aggregate dimension in the sample was 4.9 μm × 4.9 μm with a mean top surface area of 32.8 μm^2. The largest aggregate was 12.4 μm × 7.6 μm for a top surface area of 94 μm^2, which is an order of magnitude larger than a comparable aqueous kaolinite suspension without guar gum (Figure 2). The dissolved guar gum in the kaolinite suspension also affected the size distribution of the aggregates. The proportion of aggregates with stacking lengths of 1−10 μm and 10−20 μm were 78% and 22%, respectively (Figure 2b). Another experiment was made using the polysaccharide ethyl cellulose (EC) (Figure 3b). The EC sample used in this work had 48% ethoxy groups and an average number of 2.5 ethoxy groups per glucose unit. Ethyl cellulose is not soluble in water and the co-solvent, ethanol, was used. The pH of the resulting dispersion was 5.2. In the kaolinite suspension with ethyl cellulose, the mean stacking length of the aggregates was 3.6 μm, the largest aggregate was 8.0 × 5.0 μm (width × stacking length), and indicates an aggregate size increase (Figure 4b) in comparison to completely aqueous conditions. Aggregates with stacking lengths of 1−10 μm and 10−20 μm were 95% and 5%, respectively (Figure 2c). Although the size distribution of aggregates in guar gum was broader, the stacking lengths were relatively similar for both guar gum and EC treated samples. In an experiment performed to assess the relative roles of EC and ethanol in the aggregation of pH 5.5 kaolinite suspensions (Figure 5a), several aggregates were observed and the largest aggregate had an apparent surface area of 99 μm^2 (not shown). The mean stacking length was 5.4 μm and aggregates with stacking lengths of 1−10 μm and 10−20 μm were 95% and 5%, respectively (Figure 2d). The proportions of aggregate lengths were similar to EC-treated samples and indicate the potential role of ethanol alone in aggregation. A representative aggregate indicated by the white arrow (Figure 5a) had an apparent top area of 41.5 μm^2. When the kaolinite was dispersed in ethanol alone, aggregates with a booklet morphology were formed with platelets at the sides of booklets in edge-to-face interactions (Figure 5b). In addition and quite surprisingly,

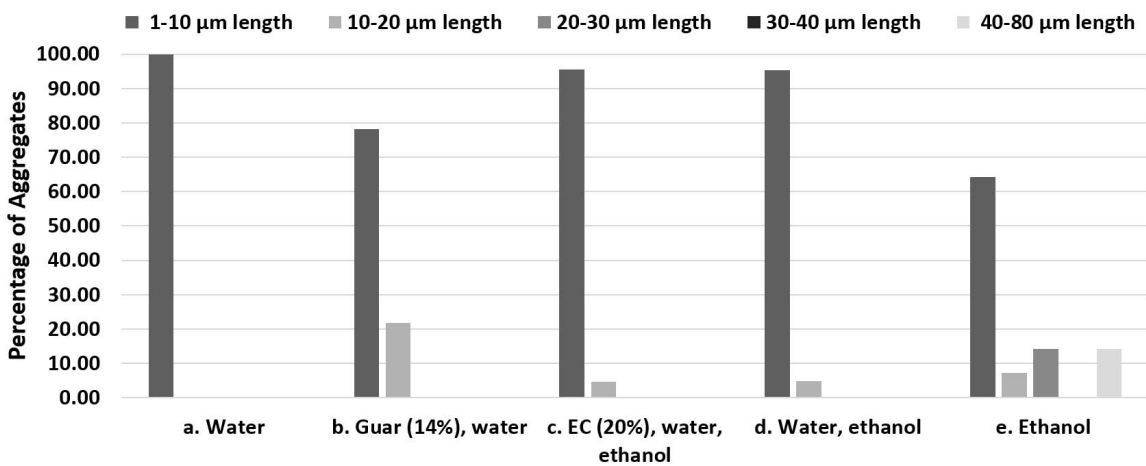

Figure 2. Size distribution histogram of kaolinite (0.3 g) aggregates dispersed in water and ethanol with and without ethyl cellulose and guar gum. The solvents or solvent mixtures used were as follows: (a, b) 15 mL of water, (c, d) 37.5 mL of water and 11.25 mL of ethanol, and (e) 6.5 mL of ethanol. The five aggregate length ranges considered were from left to right 1−10 μm, 10−20 μm, 20−30 μm, 30−40 μm, and 40−80 μm.

https://doi.org/10.1346/CCMN.2017.064059 Published online by Cambridge University Press

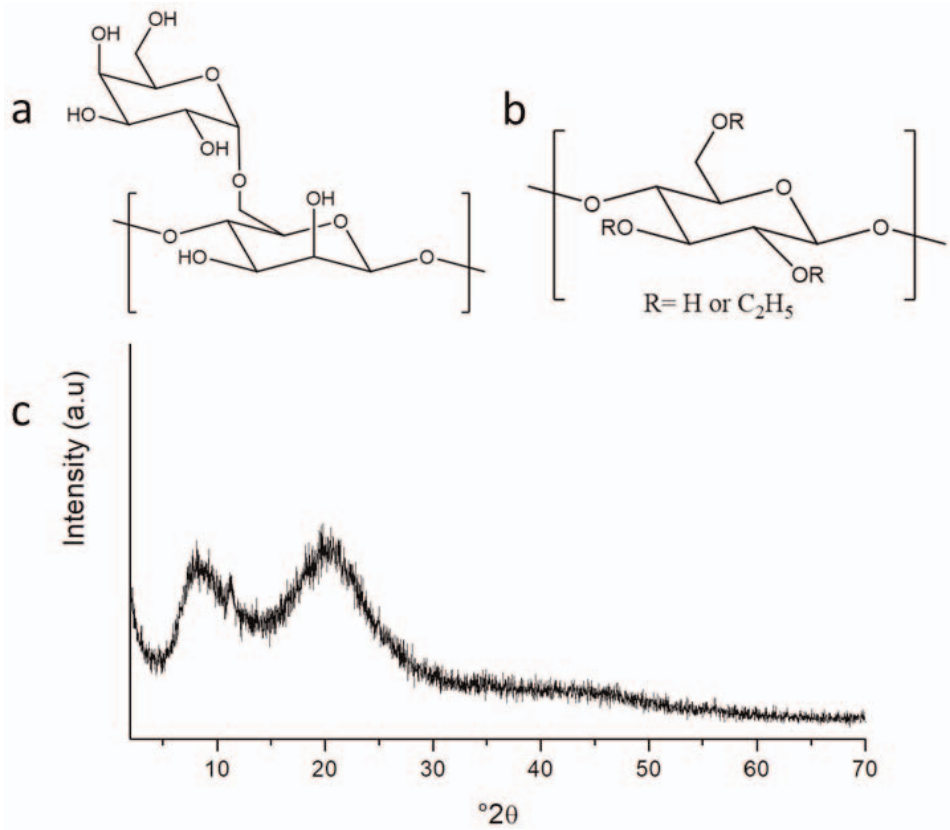

Figure 3. The chemical structures of (a) guar gum, (b) ethyl cellulose, and (c) XRD pattern of ethyl cellulose.

spectacular aggregates were observed when ethanol alone was used to disperse kaolinite (Figures 6a, 6b, 2e). The largest aggregate was 87 μm × 30 μm with a top surface area close to 3,000 μm^2. The aggregate size distribution of kaolinite dispersed in ethanol was distinctly broader than kaolinite dispersed in just water and 36% of the aggregates had stacking lengths >10 μm and 14% had stacking lengths of 40–80 μm. The mean top surface area of the aggregates was 344 μm^2, which is approximately 60 times greater than that of kaolinite

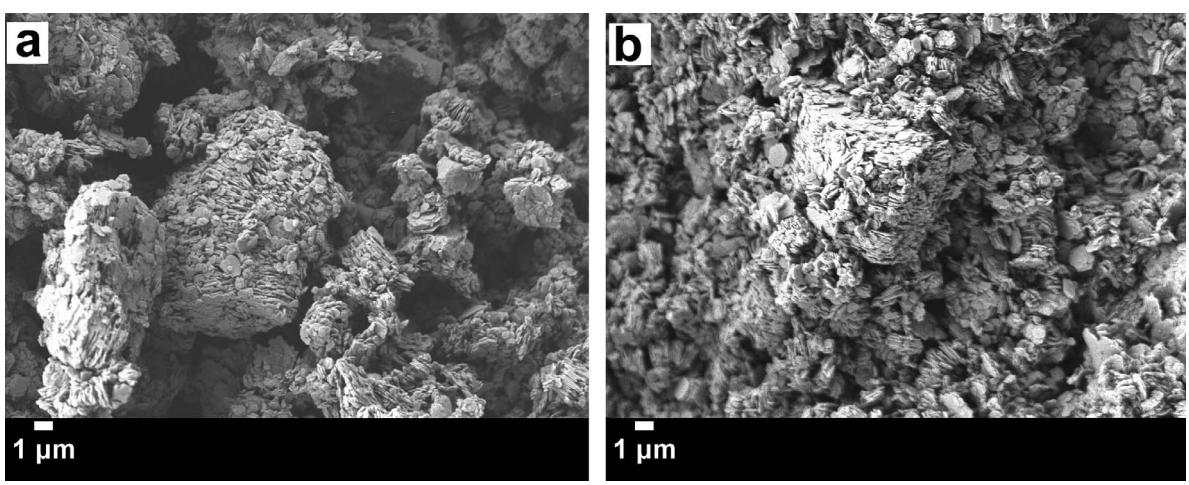

Figure 4. SEM micrographs magnified 4,000 × of kaolinite (0.3 g) dispersed in (a) 15 mL of water with 0.05 g of guar gum (86% kaolinite/14% guar gum) and (b) 37.5 mL of water, 11.25 mL of ethanol, and 0.075 g of ethyl cellulose that was previously dissolved in the ethanol (80% kaolinite/20% ethyl cellulose).

https://doi.org/10.1346/CCMN.2017.064059 Published online by Cambridge University Press

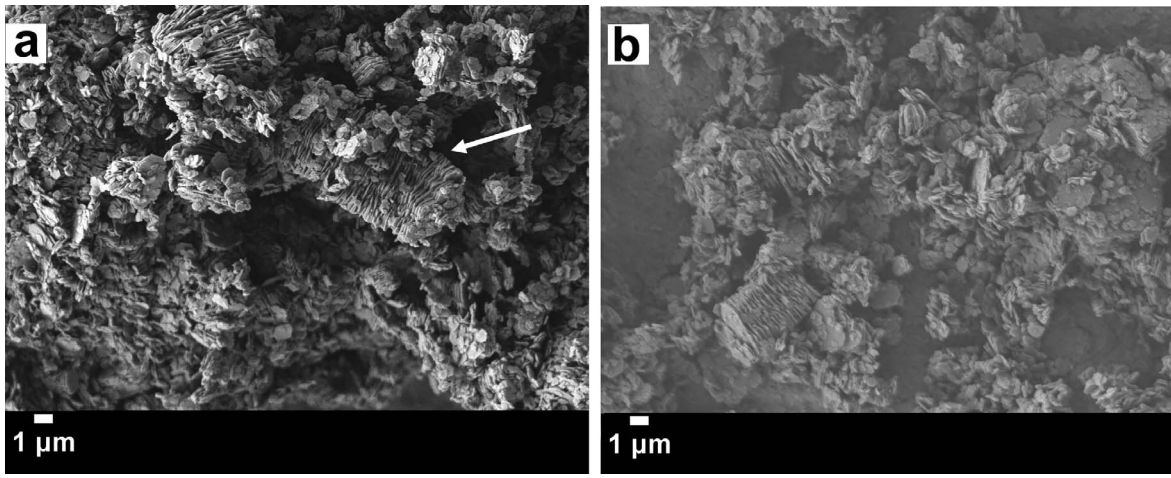

Figure 5. SEM micrographs magnified 4,000 × of kaolinite (0.3 g) dispersed in (a) 37.5 mL of water and 11.25 mL of ethanol and (b) dispersed in 6.5 mL of ethanol.

dispersed in just water. The dramatic differences between the mean top surface areas of the kaolinite sample aggregates not only reflected the increased stacking lengths of kaolinite particles dispersed in just ethanol (mean value 16 μm), but also an increased lateral aggregation of platelets into larger aggregates (mean value 8 μm) due to edge-to-edge interactions. The largest aggregate (Figure 6b) was magnified 7,000 × to reveal platelets piled together face-to-face and the piles closely arranged by edge-to-edge interactions to form the observed aggregate. On the sides, small platelets were linked to the aggregate in an edge-to-face fashion. The edge-to-edge interactions played a major role and were the driving force for the construction of aggregates with large basal surfaces. The 7,000 × magnification (Figure 6b) also revealed that the platelet thickness was quite regular and estimated to be ~50 nm, which corresponds to roughly 70 alumino-silicate layers. The 50 nm value is in very good agreement with values calculated using the Scherrer equation (Table 1). The platelets were not perfectly stacked, but had cavities between the stacks that led to porosity in the assemblies. These cavities were the result of imperfect planes and some platelets showed curvature. The observation that ethanol in the dispersion medium can induce the formation of large aggregates led to the use of other non-aqueous, non-hydroxylated solvents. Because kaolinite and illite are the major constituents of oil-sand fine fractions (Adeyinka *et al*., 2009; Osacky *et al.*, 2013), a solvent that has potential use in a non-aqueous extraction process to remove bitumen from oil sands was chosen. Cyclohexane (CH) has such a potential (Nikakhtari *et al*., 2016). The potential role of additives, such as EC, in future extraction processes was also suggested (Detellier *et al*., 2015; Lin *et al.*, 2016) and were consequently also tested. For additive solubiliza-

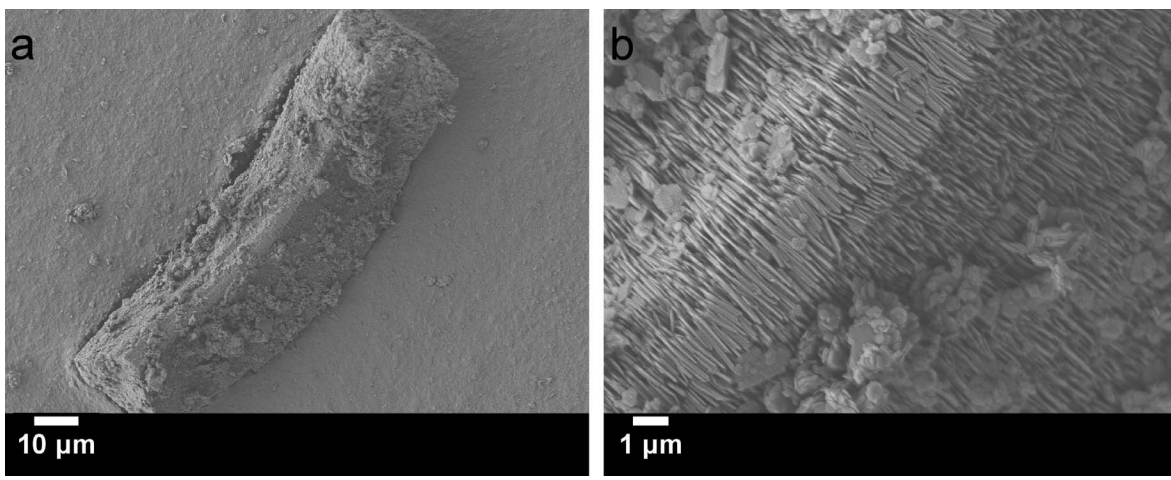

Figure 6. SEM micrographs of kaolinite (0.3 g) dispersed in 6.5 mL of ethanol magnified (a) 900 × and (b) 7,000 × .

https://doi.org/10.1346/CCMN.2017.064059 Published online by Cambridge University Press

Table 1. Full width at half maximum values (FWHM in °2θ) for the d_{001}, d_{002}, and d_{060} reflections.

Sample	FWHM (001) (°2θ)	FWHM (002) (°2θ)	FWHM (060) (°2θ)	L_{001} (nm) (n)	L_{002} (nm) (n)	CST_{060} (nm)
Kaolinite	0.21	0.22	0.36	38 (53)	37 (52)	55
After dispersion in cyclohexane and 1.5 mL of toluene	0.23	0.23	0.36	34 (48)	34 (48)	55
After dispersion in cyclohexane and 1.5 mL of EC in toluene	0.30	0.30	0.46	26 (36)	26 (36)	43
After dispersion in cyclohexane and 4.5 mL of EC in toluene	0.39	0.43	0.57	20 (28)	19 (27)	35
After dispersion in cyclohexane and 9 mL of EC in toluene	0.38	0.41	0.55	21 (29)	20 (28)	36
Physical Mixture: 0.3 g Kaolinite + 0.075 g of EC	0.23	0.23	0.38	34 (48)	34 (48)	52
Physical Mixture: 0.3 g Kaolinite + 0.225 g of EC	0.24	0.24	0.36	33 (46)	33 (46)	55
Physical Mixture: 0.3 g Kaolinite + 0.45g of EC	0.27	0.28	0.38	29 (41)	29 (41)	52
After dispersion in water (37.5 mL) and ethanol (11.25 mL)	0.28	0.27	0.36	29 (41)	29 (41)	55
After dispersion in water (37.5 mL) and ethanol (11.25 mL) with EC (0.075 g)	0.24	0.25	0.37	33 (46)	32 (45)	54
After dispersion in ethanol (6.5 mL)	0.24	0.24	0.36	33 (46)	33 (46)	55

The crystallite size (in nm) in the *c* direction (L_{001} and L_{002}) was calculated with the Scherrer equation using the d_{001} and d_{002} reflections (Morato *et al*., 2007). The coherent scattering thickness in the *b* direction (CST_{060}) was calculated using the Warren-Bodenstein equation for the d_{060} reflection (Brindley, 1980). The values are the average of two independent measurements, except for the physical mixtures. The number of layers in the individual stacks, *n*, is given in parenthesis and was obtained from L_{00l}/0.715. The ethyl cellulose (EC) concentration in toluene was 50 g/L and the amount of kaolinite was 0.3 g in all cases.

tion, a co-solvent system with 5 mL of CH and various amounts of toluene (Tol) were typically used. The co-solvent CH-Tol yielded a typical card-house structure (Figure 7a), which was quite similar to that observed in water (Figure 1). A small number of aggregates with a mean top surface area of 3.0 μm^2 and a mean stacking length of 2.0 μm (Figure 8a) was observed. A 3-fold increase in the amount of toluene increased aggregation and resulted in aggregates with a mean top surface area of 95 μm^2 and a mean stacking length of 5.0 μm (Figure 7b). Large booklet aggregates similar to those in ethanol were observed with a typical card-house structure (Figure 7b). Large aggregates were also observed in pure toluene (Figure 8b). Toluene is a planar aromatic molecule that can induce dipole-dipole interactions with kaolinite basal surfaces, produce a piling effect, and form platelet piles with a 10 μm mean aggregate width assembled edge-to-edge. The edge-to-edge assembly and the increased mean stacking length (16 μm) resulted in a relatively large mean top surface area of 284 μm^2, which is comparable to that achieved using ethanol alone (344 μm^2).

A similar effect was seen for indole solutions in toluene or heptane (Fafard *et al*., 2013). An aromatic polymer in the dispersion medium, such as polystyrene, or a polysaccharide, such as ethyl cellulose, dramatically increased aggregate size with 80% kaolinite (Figure 9) in comparison to the blank experiments (Figure 7a). The largest aggregate for the polystyrene sample was 80 μm × 27 μm and 19 μm × 10 μm for ethyl cellulose. For both polystyrene and ethyl cellulose, edge-to-face platelet organization was observed and the samples had both large aggregates and typical card house structures. Very large aggregates with apparent top surface areas of >2,000 μm^2 (57% kaolinite) and >3,000 μm^2 (40% kaolinite) were produced when relatively large ethyl cellulose and toluene concentrations were used (Figure 10) and most of the typical card-house structures disappeared at both of these kaolinite concentrations. For a kaolinite concentration of 57%, aggregates with stacking lengths of 1–10 μm were 64% (Figure 8d). When the kaolinite suspension concentration was decreased to 40%, the kaolinite aggregates with stacking lengths of 1–10 μm decreased to 42%, which reflects the dependence of aggregate size on the polymer concentration (Figure 8e). For both 40% and 57% kaolinite, approximately 21–23% of the aggregates had stacking lengths between 20 and 80 μm, which indicates that larger aggregates form when relatively large polymer concentrations are used. Face-to-face platelet piles were organized through edge-to-edge interactions into larger aggregates. The resultant superstructure organization of

https://doi.org/10.1346/CCMN.2017.064059 Published online by Cambridge University Press

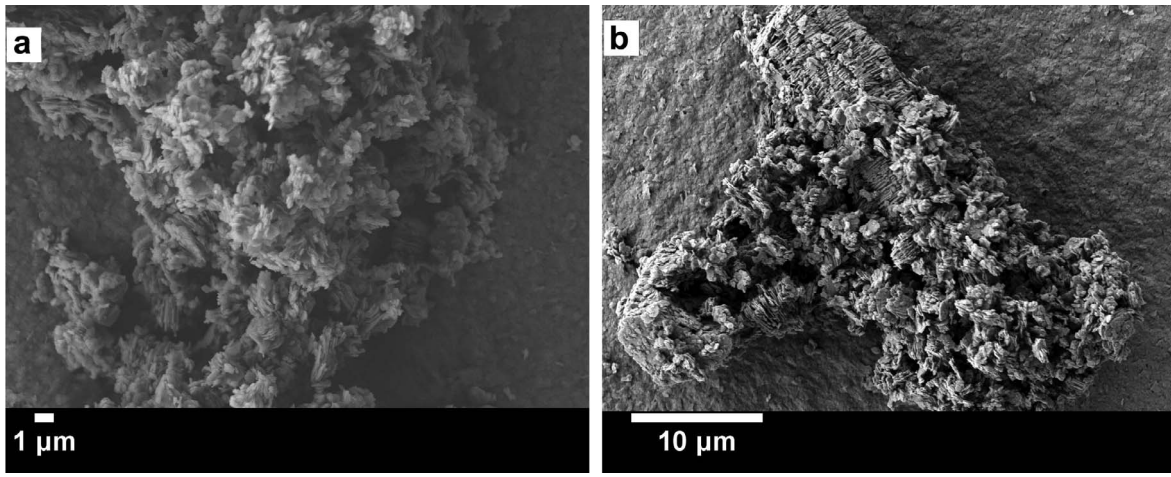

Figure 7. SEM micrographs of kaolinite (0.3 g) dispersed in (a) 5 mL of cyclohexane and 1.5 mL of toluene at 4,000 × and (b) 5 mL of cyclohexane and 4.5 mL of toluene at 2,700 × .

the clay platelets was decorated with small kaolinite particles linked edge-to-face.

An alternative experiment was devised to assess the evolution of kaolinite aggregates in EC over time. A sample with an 80:20 kaolinite to EC ratio dispersed in the co-solvent CH-Tol was analyzed along with a sample blank. For a 0 h drying period, aggregates formed both in the EC-treated sample and the blank sample. The blank sample had the same concentration of kaolinite suspended in CH-Tol without EC. The stacking length of the blank was consistent over drying periods of 0, 4, and 7 h and the mean stacking length was 9.5±0.5 µm. In contrast, kaolinite suspensions with EC dried for 4 h had ~42% greater stacking lengths (7.9 µm to 11.2 µm) and the stacking length increased another 9% with further drying until a 12.2 µm mean stacking length was reached after 7 h.

Visual analysis of the SEM images revealed a fibrous morphology (arrow, Figure 11b) which indicated some segregation of kaolinite and EC domains at 0 h. After drying for 4 and 7 h, however, a network between clay platelets and aggregates formed and was particularly dominant after 7 h of drying (Figures 11d and 11f). Thus, during the 4- and 7-h drying, the polymer segments were distributed over the clay platelets to lend a cohesive appearance to the platelets and aggregates. The mean stacking lengths and a visual assessment indicated that the polymer-clay surface

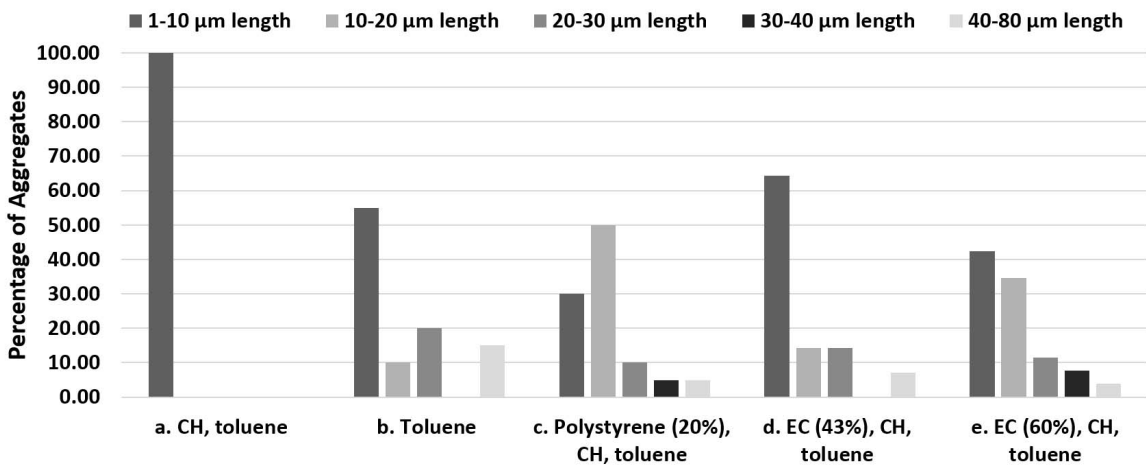

Figure 8. Size distribution histogram of aggregates of kaolinite (0.3 g) in non-aqueous solvents with and without polystyrene and ethyl cellulose (EC). The following non-aqueous solvents or solvent mixtures were used: (a) 5 mL of cyclohexane and 1.5 mL of toluene, (b) 6.5 mL of toluene, (c) 5 mL of cyclohexane and 1.5 mL of toluene, (d) 5 mL of cyclohexane and 4.5 mL of toluene, and (e) 5 mL of cyclohexane and 9 mL of toluene. The five aggregate length ranges considered were from left to right 1−10 µm, 10−20 µm, 20−30 µm, 30−40 µm, and 40−80 µm.

https://doi.org/10.1346/CCMN.2017.064059 Published online by Cambridge University Press

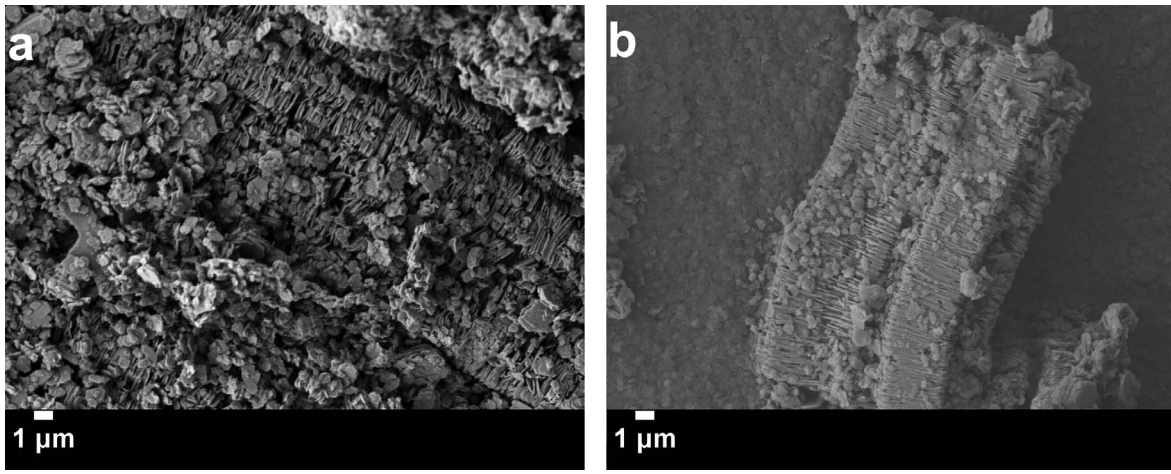

Figure 9. SEM micrographs of kaolinite (0.3 g) aggregates dispersed in 5 mL of cyclohexane and 1.5 mL of toluene (a) with 0.075 g of polystyrene magnified 4,000 × and (b) with 0.075 g ethyl cellulose magnified 3,700 × .

interactions were augmented as the EC concentration was increased during sample drying. The aggregate widths increased with increased drying time for both the solvent-only and the EC-treated samples. In the blank and EC-treated samples, the mean aggregate width at 0 h drying were, respectively, 5.6 μm and 5.1 μm and increased to 8.0 μm and 7.2 μm after 7 h drying. For both 0- and 7-h drying, increases in the mean width were steady and comparable over time and reflect enhanced edge-edge interactions that occurred with or without EC. Increases in aggregate surface area for both the blank and EC-treated samples were measured over time. After 4- and 7-h drying, the EC-treated sample aggregates had mean surface areas of 93 μm^2 and 118 μm^2 or surface area increases of about 57% and 32%, respectively, in comparison to the solvent-only sample aggregates. An X-ray diffraction pattern of ethyl cellulose had two very broad diffraction lines centered approximately at 8.5º2θ and 20.6º2θ, similar to values reported in the literature (Balköze *et al*., 2014) (Figure 3c). The 8.5º2θ and 20.6º2θ peaks correspond, respectively, to the 10.4 Å interchain and the 4.3 Å intrachain distances observed in Figures 12d and 12e, albeit with smaller intensities, particularly for the 8.5º2θ region. The reduced intensities could be due to partial loss of interchain ordering that resulted from shaking the kaolinite in a non-aqueous solvent. X-ray diffraction peak broadening for kaolinite suspensions with EC was readily observed in the materials that were shaken in non-aqueous solvents and subsequently dried (Figures 12c, 12d, 12e). Physical mixtures with the same relative quantities of kaolinite and EC did not have similar X-ray peak broadening and

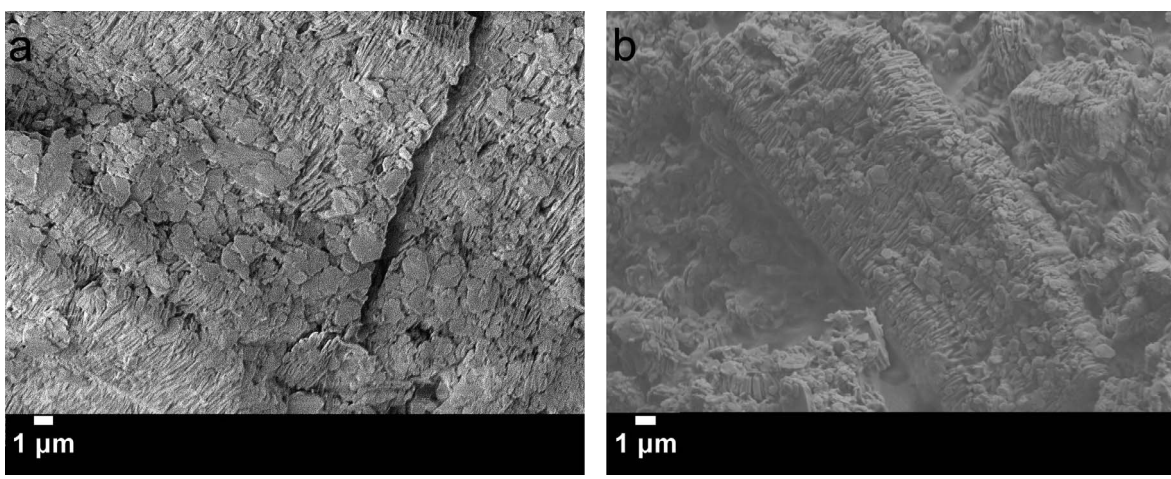

Figure 10. SEM micrographs of kaolinite (0.3 g) dispersed in (a) 5 mL of cyclohexane, 4.5 mL of toluene, and 0.225 g of ethyl cellulose magnified 4,000 × and (b) dispersed in 5 mL of cyclohexane, 9 mL of toluene, and 0.45 g of ethyl cellulose magnified 4,300 × .

https://doi.org/10.1346/CCMN.2017.064059 Published online by Cambridge University Press

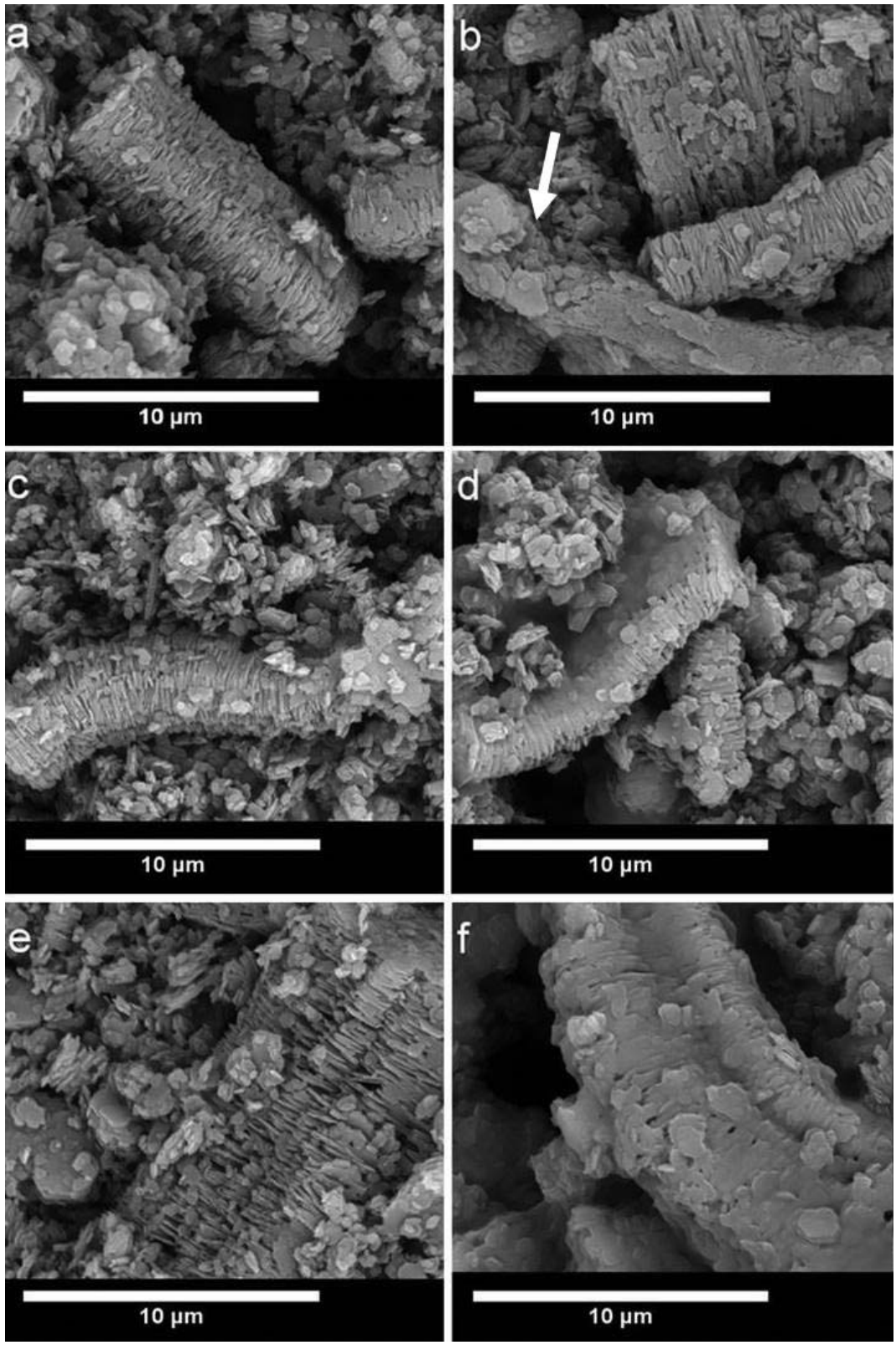

Figure 11. SEM micrographs (10,000 ×) of kaolinite (0.3 g) dispersed in 5 mL of cyclohexane after (a) 0 h drying, (b) 0 h drying with 0.075 g ethyl cellulose, (c) 4 h drying, (d) 4 h drying with 0.075 g ethyl cellulose, (e) 7 h drying, and (f) 7 h drying with 0.075 g ethyl cellulose.

https://doi.org/10.1346/CCMN.2017.064059 Published online by Cambridge University Press

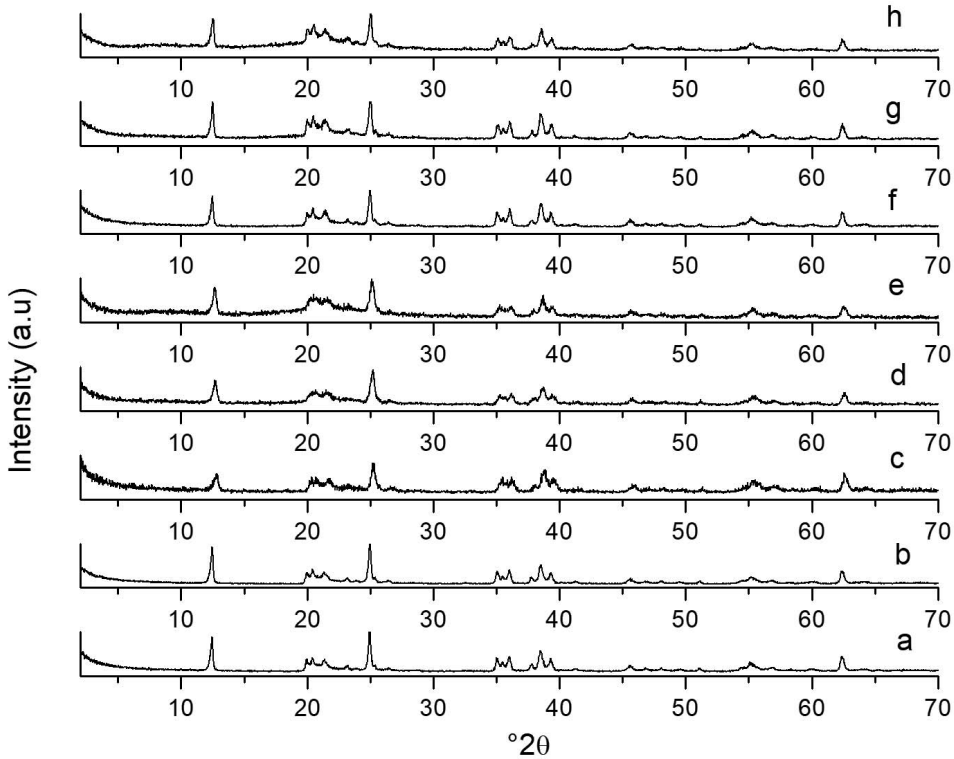

Figure 12. XRD patterns of kaolinite (a), and kaolinite (0.3 g) dispersed in (b) 5 mL of cyclohexane and 1.5 mL of toluene, (c) 5 mL of cyclohexane and 1.5 mL of ethyl cellulose in toluene, (d) 5 mL of cyclohexane and 4.5 mL of ethyl cellulose in toluene, (e) 5 mL of cyclohexane and 9 mL of ethyl cellulose in toluene, and kaolinite (0.3 g) physically mixed with (f) 0.075 g of ethyl cellulose, (g) 0.225 g of ethyl cellulose, and (h) 0.45 g of ethyl cellulose.

this discounts the possibility that the peak broadening can be attributed to sample transparency produced by EC (Figures 12f, 12g, 12h). When the kaolinite was dispersed in solvents without EC, no obvious peak broadening occurred (Figure 12b). A particle size analysis of the kaolinite was calculated on the 001 and 002 reflections using the Scherrer equation and a shape factor of 0.89 (Morato *et al*., 2017), and on the *060* reflection (Franco *et al*., 2004) using the Warren-Bodenstein equation (Warren and Bodenstein, 1966; Brindley, 1980). The full width at half maximum (FWHM) values were not corrected for instrumental effects (Eberl *et al*., 1996) because the small size of the kaolinite particles in the aggregates yields relatively large FWHM values. The FWHM of the 001 and 002 diffraction peaks were almost identical, led to the same crystal thickness (L_{001}) values, and validated the approach used to calculate the number of stacked layers in a platelet as L/d_{001} (Brindley, 1980) (Table 1). The average kaolinite platelet thickness was 38 nm, which corresponds to 53 layers and is in the range of values previously reported (Johnston, 2010).

After kaolinite was dispersed in the cyclohexane/toluene solvent mixture, platelet size remained about the same. When EC was added to the solvent mixture, however, the L_{001} value and the number of layers in platelets were dramatically reduced to almost half the value for the solvent mixture without EC. In contrast, the effect was much less pronounced for physical mixtures of kaolinite and EC and the number of layers remained between 40 and 50. A number of kaolinite samples were dispersed in water, ethanol, and various water/ethanol binary mixtures, but the FWHM (001, 002, and 060) values were not affected. The FWHM values were also not affected by EC or guar gum in aqueous systems. The most plausible interpretation is that EC-kaolinite surface interactions in non-aqueous media can interfere with the layer stacking process and result in smaller stacks linked together by EC layers, which act as a cement between the bricks of kaolinite platelets to construct the large aggregates observed using SEM. Interestingly, the coherent scattering thickness (CST) in the 060 direction was also reduced from 55 nm to 35 nm and indicates that EC interacted with the edges of the platelets. This could be the basis for the edge-edge lateral piling of the stacked platelets seen in the SEM images. In strong contrast in aqueous systems, the network of water H-bonds around kaolinite platelets competed successfully with potential EC-kaolinite surface interactions and no large aggregates formed or were seen in SEM images.

The FTIR-ATR spectra were recorded for a variety of kaolinite suspension systems. Because the absorption peak is broad, no significant shift in the OH bond stretching vibrations was observed. This was expected

https://doi.org/10.1346/CCMN.2017.064059 Published online by Cambridge University Press

because the XRD data showed interchain reflections, the EC remained aggregated, and the network of EC H-bonds was not significantly modified by interactions with the kaolinite platelets.

CONCLUSIONS

This approach to understanding kaolinite aggregates was based on SEM observations of solids formed by the slow evaporation of solvents from kaolinite suspensions. It should be stressed that the morphology of kaolinite suspended in solvents was not necessarily what was observed in the SEM images of solid materials after the solvent was dried. Instead, the SEM images showed the resulting assembly process during slow solvent evaporation. The experimental procedure was rigorously identical in all the cases and, consequently, the SEM images compared how platelets can interact in various media and lead to different morphologies under different environments. Quite spectacular differences in morphology were indeed observed between aqueous and non-aqueous samples, particularly when organic polymers were dissolved in the organic solvent. Ethyl cellulose (EC), an etherified polysaccharide, played a dual role by aggregating the platelets and reducing the number of stacked layers in each platelet. A plausible effect of EC was to link kaolinite platelets together into face-to-face piles which are stacked edge-edge. This was also observed when other polymers, such as polystyrene (Figure 9a) and polycaprolactone diol, were used (not shown). Organic solvents that can interact with silanol or aluminol groups can play a similar role, but to a smaller extent. The length of time used to dry kaolinite suspensions also played a role in aggregate formation for suspensions with polymers. One could generalize, even if perhaps prematurely, that organic moieties that can associate and chemically interact with silanol and/or aluminol groups can bring kaolinite particles together, particularly in non-aqueous media. Future interpretations of catalytic reactions that occur in non-aqueous media with kaolinite as a catalyst or as a catalyst support will need to take these aggregates into consideration. Additionally, further research might shed definitive insight into potential applications of particularly large aggregates by correlating the aggregates to characteristics that depend on morphology, such as mechanical, thermal, and permeation properties. In future non-aqueous bitumen extraction processes, large aggregates formed by the use of selected polymers dissolved in the suspension solvent could become of great importance in the sedimentation of residual fine particles.

ACKNOWLEDGMENTS

The authors are grateful to the University of Alberta Institute for Oil Sands Innovation (IOSI) for providing research funding. They are grateful also to the Natural Sciences and Engineering Research Council of Canada (NSERC) for a Discovery Grant. The Canada Foundation for Innovation and the Ontario Research Fund are gratefully acknowledged for infrastructure grants to the University of Ottawa Center for Catalysis Research and Innovation.

REFERENCES

Adeyinka, O.B., Samiei, S., Xu, Z., and Masliyah, J.H. (2009) Effect of particle size on the rheology of Athabasca clay suspensions. *Canadian Journal of Chemical Engineering*, **87**, 422–434.

Aung, L.L., Tertre, E., and Petit, S. (2015) Effect of the morphology of synthetic kaolinites on their sorption properties. *Journal of Colloid and Interface Science*, **443**, 177–186.

Balköse, D., Horak, D., and Soltès, L. (2014) *Key Enginering Materials, Vol. 1: Current State-of-the-Art on Novel Materials*. CRC Press, Boca Raton, Florida, USA, pp. 445–446.

Beaufort, D., Cassagnabere, A., Petit, S., Lanson, B., Berger, G., Lacharpagne, J.C., and Johansen, H. (1998) Kaolinite-to-dickite reaction in sandstone reservoirs. *Clay Minerals*, **33**, 297–316.

Brack, A. (2013) Clay minerals and the origin of life. Chapter 10, pp. 507–522 in: *Handbook of Clay Science, 2nd Edition; Developments in Clay Science, Volume 5, Part A*. (F. Bergaya and G. Lagaly, editors). Elsevier, Amsterdam.

Brigatti, M.F., Galán, E., and Theng, B.K.G. (2013) Structure and mineralogy of clay minerals. Chapter 2, pp. 29–35 in: *Handbook of Clay Science, 2nd Edition; Developments in Clay Science, Volume 5, Part A*. (F. Bergaya and G. Lagaly, editors). Elsevier, Amsterdam.

Brindley G.W. (1980) Order-disorder in clay mineral structures. Chapter 2, pp. 125–195 in: *Crystal Structures of Clay Minerals and their X-ray Identification* (G.W. Brindley and G. Brown, editors). Mineralogical Society, London.

Christidis, G.E. (2013) Assessment of industrial clays. Chapter 4, pp. 425–450 in: *Handbook of Clay Science, 2nd Edition; Developments in Clay Science, Volume 5, Part A*. (F. Bergaya and G. Lagaly, editors). Elsevier, Amsterdam.

Dedzo, G.K. and Detellier, C. (2016) Functional nanohybrid materials derived from kaolinite. *Applied Clay Science*, **130**, 33–39.

Detellier, C. and Schoonheydt, R.A. (2014) From platy kaolinite to nanorolls. *Elements*, **10**, 201–206.

Detellier, C., Letaief, S., Fafard, J., and Dedzo, G.K. (2015) Desorption of bitumen from clay particles and mature fine tailings, U.S. Patent application No 14/083,824; US 2015/0136651 A1: published May 21, 2015.

Dziadkowiek, J., Mansa, R., Quintela, A., Rocha, F., and Detellier, C. (2017) Preparation, characterization and application in controlled release of Ibuprofen-loaded guar gum/Montmorillonite bionanocomposites. *Applied Clay Science*, **135**, 52–63.

Eberl, D.D., Drits, V., Srodon, J., and Nüesch, R. (1996) MudMaster: A program for calculating crystallite size distributions and strain from the shapes of X-ray diffraction peaks. *US Geological Survey Open File Report*, 96.171, 44.

Fafard, J., Lyubimova, O., Stoyanov, S.R., Dedzo, G.K., Gusarov, S., Kovalenko, A., and Detellier, C. (2013) Adsorption of indole on kaolinite in non-aqueous media: organoclay preparation and characterization, and 3D-RISM-KH molecular theory of solvation investigation. *Journal of Physical Chemistry, C*, **117**, 18556–18566.

Franco, F., Pérez-Maqueda, L.A., and Pérez-Rodriguez, J.L. (2004) The effect of ultrasound on the particle size and structural disorder of a well-ordered kaolinite. *Journal of Colloid and Interface Science*, **274**, 107–117.

Galimberti, M., Cipolletti, V.R., and Coombs, M. (2013) Applications of clay-polymer nanocomposites. Chapter 4, pp. 539–586 in: *Handbook of Clay Science, 2nd Edition; Developments in Clay Science, Volume 5, Part A*. (F. Bergaya and G. Lagaly, editors). Elsevier, Amsterdam.

Giese, R.F. (1982) Theoretical studies of the kaolin minerals – electrostatic calculations. *Bulletin de Minéralogie*, **105**, 417–424.

Gupta, V., Hampton, M.A., Stokes, J.R., Nguyen, A.V., and Miller, J.D. (2011) Particle interactions in kaolinite suspensions and corresponding aggregate structures. *Journal of Colloid and Interface Science*, **359**, 95–103.

Hu, Y., Liu, L., Min, F., Zhang. M., and Song, S. (2013) Hydrophobic agglomeration of colloidal kaolinite in aqueous suspensions with dodecylamine. *Colloids and Surfaces A: Physicochem. Engineering. Aspects*, **434**, 281–286.

Johnston, C.T. (2010) Probing the nanoscale architecture of clay minerals. *Clay Minerals*, **45**, 245–279.

Kameda J., Saruwatari K., Beaufort D., and Kogure T. (2008) Textures and polytypes in vermiform kaolins diagenetically formed in a sandstone reservoir: A FIB-TEM investigation. *European Journal of Mineralogy*, **20**, 199–204.

Laszlo, P. (1986) Catalysis of organic reactions by inorganic solids. *Accounts of Chemical Research*, **19**, 121–127.

Lin, F., He, L., Hou, J., Masliyah, J., and Xu, Z. (2016) Role of ethyl cellulose in bitumen extraction from oil sands ores using an aqueous-nonaqueous hybrid process. *Energy & Fuels*, **30**, 121–129.

Liu, J., Gaikwad, R., Hande, A., Das, S., and Thundat, T. (2015a) Mapping and quantifying surface charges on clay nanoparticles. *Langmuir*, **31**, 10469–10476.

Liu, J., Lin C., and Miller, J.D. (2015b) Simulation of cluster formation from kaolinite suspensions. *International Journal of Mineral Processing*, **145**, 38–47.

Liu, X., Lu, X., Sprik, M., Cheng, J., Meijer, E.J., and Wang, R. (2013) Acidity of edge surface sites of montmorillonite and kaolinite. *Geochimica et Cosmochimica Acta*, **117**, 180–190.

Mansa, R. and Detellier, C. (2013) Preparation and characterization of guar-montmorillonite nanocomposites. *Materials*, **6**, 5199–5216.

Mccabe R.W. and Adams, J.M. (2013) Clay minerals as catalysts. Chapter 4, pp. 491–523 in: *Handbook of Clay Science, 2nd Edition; Developments in Clay Science, Volume 5, Part A*. (F. Bergaya and G. Lagaly, editors). Elsevier, Amsterdam.

Moll, Jr., W.F. (2001) Baseline studies of The Clay Minerals Society source clays: geological origin. *Clays and Clay Minerals*, **49**, 374–380.

Morato, A. and Rives, V. (2017) Comments on the application of the Scherrer equation. *Applied Catalysis B: Environmental*, **202**, 418–419.

Murray, H.H. and Keller, W.D. (1993) Kaolins, kaolins, and kaolins. Pp 1–24 in: *Kaolin Genesis and Utilization, Special Publication No 1* (H.H. Murray, W.M. Bundy, and C.C. Harvey, editors). The Clay Minerals Society, Boulder, Colorado, USA.

Ngnie, G., Dedzo, G.K., and Detellier, C. (2016) Synthesis and catalytic application of palladium nanoparticles supported on kaolinite-based nanohybrid materials. *Dalton Transactions*, **45**, 9065–9072.

Nikakhtari, H., Pal, K., Wolf, S., Choi, P., Liu, Q., and Gray, M.R. (2016) Solvent removal from cyclohexane-extracted oil sands gangue. *Canadian Journal of Chemical Engineering*, **94**, 408–414.

Osacky, M., Geramian, M., Ivey, D.G., Liu, Q., and Etsell, T.H. (2013) Mineralogical and chemical composition of petrologic end members of Alberta oil sands. *Fuel*, **113**, 148–157.

Pruett, R.J. and Webb, H.L. (1993) Sampling and analysis of KGa-1b well-crystallized kaolin source clay. *Clays and Clay Minerals*, **41**514–519.

Psyrillos, A., Howe, J.H., Manning, D.A.C., and Burley, S.D. (1999) Geological shape and controls on kaolin particle and consequences for mineral processing. *Clay Minerals*, **34**, 193–208.

Rebertus, R.A., Weed, S.B., and Buol, S.W. (1986) Transformations of biotite to kaolinite during saprolite-soil weathering. *Soil Science Society of America Journal*, **50**, 810–819.

Schroeder, P.A. and Erickson, G. (2014) Kaolin: from ancient porcelains to nanocomposites. *Elements*, **10**, 177–182.

Srivastava, M. and Kapoor, V.P. (2005) Seed gallactomannans: An overview. *Chemistry & Biodiversity*, **2**, 295–317.

Warren, B.E. and Bodenstein, P. (1966). The shape of two-dimensional carbon black reflections. *Acta Crystallographica*, **20**, 602–605.

Wilson, M.J., Wilson, L., and Patey, I. (2014) The influence of individual clay minerals on formation damage of reservoir sandstones: a critical review with some new insights. *Clay Minerals*, **49**, 147–164.

Yong, R.N. and Mourato, D. (1990) Influence of polysaccharides on kaolinite structure and properties in a kaolinite-water system. *Canadian Geotechnical Journal*, **27**, 774–788.

(*Received 7 September 2016; revised 16 June 2017; Ms. 1133; AE: H. Dong*)